Journal of The Electrochemical Society

Reversible Long-Term Operation of a MK35x Electrolyte-Supported Solid Oxide Cell-Based Stack

To cite this article: Matthias Riegraf *et al* 2024 *J. Electrochem. Soc.* **171** 104505

Journal of The Electrochemical Society, 2024 **171** 104505

Reversible Long-Term Operation of a MK35x Electrolyte-Supported Solid Oxide Cell-Based Stack

Matthias Riegraf,[1,z] Patric Szabo,[1] Michael Lang,[1] Rémi Costa,[1] Stefan Rothe,[2] Stefan Megel,[2] and Mihails Kusnezoff[2]

[1]*German Aerospace Centre (DLR), Institute of Engineering Thermodynamics, 70569 Stuttgart, Germany*
[2]*Fraunhofer Institute of Ceramic Technologies and Systems (IKTS), 01277 Dresden, Germany*

High-temperature reversible solid oxide cells (rSOC) combine electrolyzer and fuel cell in one process unit which promises economic advantages with unrivaled high electrical efficiencies. However, large temperature gradients during dynamic rSOC operation can increase the risk of mechanical failure. Here, the degradation behavior of a 10-cell stack of the type "MK35x" with chromium-iron-yttrium (CFY) interconnects and electrolyte-supported cells (ESC) developed at Fraunhofer IKTS was investigated in rSOC operation at DLR. Its degradation was evaluated during nominal rSOC operation for more than 3400 h with 137 switching cycles between solid oxide fuel cell and solid oxide electrolysis cell operation of 24 h reflecting intermittent availability of solar energy. The voltage degradation rates of +0.58%/kh and −1.23%/kh in electrolysis and fuel cell operation, respectively, are among the lowest reported in literature. Comparison to a previously published long-term test in steam electrolysis did not show any indication for an increased degradation. Electrochemical impedance spectroscopy measurements were performed for all repeat units to evaluate the degradation behavior in detail. An overall polarization resistance decrease due to an improvement of the oxygen electrode was observed during electrolysis operation but was absent during fuel cell operation.
 [DOI: 10.1149/1945-7111/ad8036]

Manuscript submitted May 6, 2024; revised manuscript received July 26, 2024. Published October 7, 2024.

Supplementary material for this article is available online

The progressing increase of the share of intermittently available renewable energy sources (RES) in the world's electricity mixes necessitates the deployment of efficient and inexpensive energy storage and conversion technologies.[1] One promising approach, especially for seasonal energy storage, is the production of hydrogen via electrolysis technologies in times of RES curtailment and the conversion of hydrogen to electricity by means of fuel cells in times of unavailability of RES.[2] High-temperature reversible solid oxide cells (rSOC) allow to combine electrolyzer and fuel cell in one device which promises economic advantages and reduced space requirements since their use only requires one stack module that can be operated with a high capacity factor. In addition, compared to other fuel cell and electrolyzer technologies, solid oxide cells (SOC) offer by far the highest electrical efficiencies in both operating modes due to its inherent thermodynamic and kinetic advantages. Particularly high system efficiencies of solid oxide electrolysis cell (SOEC) reactors can be reached when a high-temperature heat source is available which can be used for water evaporation.[3] One option would be the coupling of an SOC to a solar thermal power plant, where during the day hydrogen is produced in electrolysis mode with the input of superheated steam and/or electricity, and during the night electricity is generated in solid oxide fuel cell (SOFC) operation from the stored hydrogen.[4]

SOC technologies aimed at dedicated operation in only fuel cell or electrolysis mode, respectively, now reach the lifetimes required for commercialization and numerous large projects up to the MW scale have been announced in recent years.[5] However, reversible solid oxide cell (rSOC) technology is still at a lower technology readiness level (TRL) of ∼5 with the largest validated installation being a 150 kW_{AC} system developed by Sunfire.[6] Current problems are the more complex balance-of-plants (BoP) component requirements and large temperature changes within the SOC stack that are caused by the switching between the two operating modes. Since SOC contain brittle ceramic components with different thermal expansion coefficients, such temperature changes are expected to increase the risk of mechanical failure. However, so far only few experimental investigations have been carried out for more than 1000 h on either cell and stack level and it is unclear to which extent rSOC operation really affects SOC lifetime.[6–11]

The IKTS has developed the MK35x stack platform developed which is based on electrolyte supported cells (ESC) and chromium-iron-yttria (CFY) interconnects.[11–17] Previous tests have shown an average voltage decrease of 0.7%/kh in SOFC for more than 20,000 h and an improvement of stack performance by +0.3%/kh after operation for more than 3000 h in solid oxide electrolysis.[14,18]

In this study, the durability of an MK35x stack was investigated in detail in rSOC operation for more than 3400 h to obtain a detailed understanding of the degradation behavior of the individual repeat units (RUs) in the stack.

Experimental

A Mk35x stack with 10 RUs and with metallic CFY(∼94 mol% Cr, 5 mol% Fe, ∼1 mol% Y_2O_3) interconnects developed by IKTS was investigated.[11–13,15,17,18] The stack had a cross flow design with internal fuel gas and open air manifolds. The CFY interconnects had a footprint area of 13.0 × 15.0 cm^2 and the active area of the ESC was 11.0 × 11.5 cm^2 (∼127 cm^2). The ESCs were based on 10 mol % Sc_2O_3–1 mol% CeO_2–89 mol% ZrO_2 (10Sc1CeSZ) electrolytes and employed $La_{1-x}Sr_xMn_{1-y}M'_yO_{3-\delta}$ (LSMM′, with M′ being a transition metal)/Sc_2O_3 stabilized ZrO_2 (ScSZ) oxygen and Ni/Gadolinium-doped ceria (CGO) electrodes (type "IKTS-G5b") developed for electrolysis operation.[19] For contacting the interconnect to the fuel electrode, nickel meshes were used. The oxygen electrode contact to the interconnect is realized using electronically conducting ceramic pastes. The stacks were sealed, commissioned (NiO reduced to metallic Ni) and pre-tested at IKTS.[17] For electrochemical stack operation at DLR Pt wires were spot welded to each CFY interconnect as voltage probes.

The numbering of the 10 RUs was upwards from the bottom. Temperatures were montored inside the external air manifolds at the inlet and the outlet, and at three different positions inside the stack (T_1 in RU 1, T_4 in RU 4, T_{10} in RU 10). The three thermocouples were inserted into the air channels until the middle position of the stack. In the following, the temperature $T_{air,\ out}$ inside the air outlet

[z]E-mail: Matthias.Riegraf@dlr.de

manifold is referred to as stack temperature unless stated otherwise. All gases were supplied via mass flow controllers.

After heat-up with 2 K min^{-1}, the gas-tightness of all RUs was monitored at an air outlet temperature of 770 °C and a dry fuel gas mixture of 40% H_2/60% N_2. A total air flow rate of 20 L min^{-1} (NLPM) was used for all tests described in the following. An initial performance characterization was carried out by performing electrochemical impedance spectroscopy (EIS) measurements at three operating points, one nominal full load operating point (FCNL) in fuel cell mode and two in electrolysis mode at nominal load (ELNL) and part load (ELPL) to enable comparison with our previous work described in Ref. 18.

In SOFC operation, a feed gas with a composition of 40% H_2, 60% N_2 with a total flow rate of 8 NLPM and a current density of 0.275 A cm^{-2} corresponding to a fuel utilization (FU) of 75% was used. The oven temperature was set to 749 °C in order to reach an air outlet temperature of 835 °C and was kept constant during the initial characterization at all operating points and during the reversible long-term test.

In electrolysis, the stack was firstly characterized at the part load operating point ELPL with a current density of −0.39 A cm^{-2} and with a total fuel gas flow rate of 5.78 NLPM (80%H_2O + 20%H_2) corresponding to a steam conversion (SC) of 75%. Then, the stack was characterized at the nominal electrolysis operating point ELNL before starting the reversible operation. An inlet fuel gas composition of 80% H_2O and 20% H_2, with a total fuel gas flow rate of 8.99 NLPM and a current density of −0.6 A cm^{-2} was used corresponding to a SC of 75%. With these operating conditions, the current-voltage characteristics (*i-V* curve) of the cell was investigated in electrolysis as well. For this purpose, starting from open circuit voltage (OCV), the current density was slowly increased by 26 mA cm^{-2} h^{-1} until a maximum value of −0.63 A cm^{-2} was reached. Then, the current density was held for 1 h and slowly decreased back to 0 A with the same rate. Additionally, in order to investigate the quality of the electrical contact resistances, the ohmic resistance was determined by EIS at OCV in the absence of a temperature gradient with a fuel gas of 20% H_2, 80% H_2O and an oven temperature of 749 °C.

After initial characterization, a long-term degradation test was started in reversible operation with a total 137 daily SOFC/SOEC cycles for overall 3850 h. During this time, the stack had to be cooled down twice after 3000 h and 3340 h after the start of the experiment for 64 h and 340 h, respectively, due to technical maintenance. Thus, the total nominal reversible operation time was 3446 h. The duration of a full SOFC/SOEC cycle was 24 h and consisted of 11 h SOFC operation, 7 h SOEC operation and the transition periods of 3 h, respectively, as depicted in Fig. 1 (top panel). Fuel gas mixtures of 80% H_2, 20%H_2O and 80% H_2O, 20% H_2 with a current density of 0.275 A cm^{-2} and −0.75 A cm^{-2} were used in SOFC and SOEC operation, respectively. In both cases, a FU or SC, respectively, of 75% was used. The SOFC operating point did not coincide with the nominal full load operating point FCNL generally used (see above) and instead of a dry fuel gas, 20% steam was added. This allowed a continuous operation of the humidifier which decreased the risk of pressure spikes while switching on the humidifier.

After the end of the reversible test, a final characterization of the stack performance was performed. The stack was electrochemically analyzed by EIS at the three reference points described above. In addition, in order to correct for degradation-related temperature changes within the stack the voltage at the nominal load SOFC operating point FCNL was investigated with an adjustment of the oven temperature so that the air outlet temperature reached 835 °C.

EIS measurements were performed with an electrochemical workstation IM 6 that was connected to the electronic load "EL1000" (Zahner-Elektrik GmbH & CO. KG, Kronach, Germany) using a voltage supply in the current circuit for electrolysis measurements. An alternating current (AC) amplitude of 0.03 A cm^{-2} with a frequency range of 20 mHz to 20 kHz was used in electrolysis, whereas in SOFC operation an amplitude of 0.015 A cm^{-2} was applied. The electrical current probes were attached to the top and bottom plates, while the voltage probes were attached at each RU of the stack enabling EIS measurements at all RUs. The analysis of the impedance spectra with an equivalent circuit model (ECM) was performed with the software ZView.

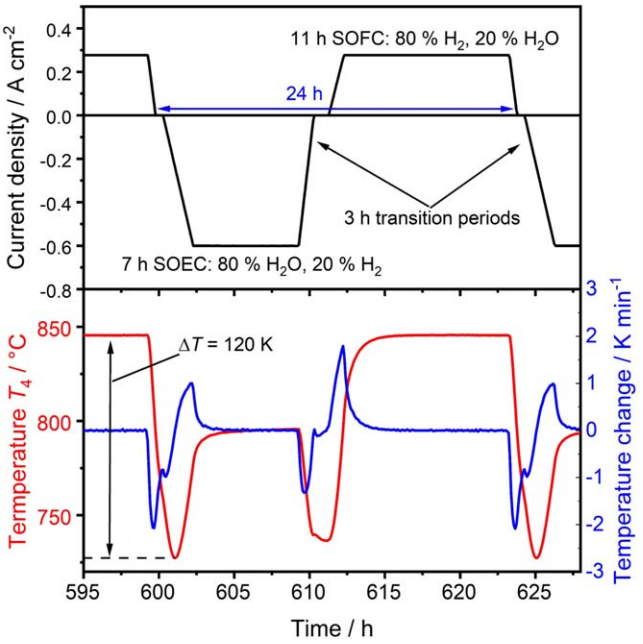

Figure 1. (Top) Operating profile during the reversible long-term test. (Bottom) Temperature changes during a representative SOFC/SOEC cycle. The data sampling rate was 0.2 min^{-1}.

Results and Discussion

In Fig. 2, the voltage and air outlet temperature evolution of the stack during the entire lifecycle of approximately 4500 h is shown. No additional conditioning of the stack was performed. During the first ∼350 h, an initial electrochemical characterization was carried out as described in the following subsection. Then, a long-term degradation test in rSOC operation over 3446 h was performed during which the stack was exposed to two thermal cycles that interrupted the rSOC durability test due to technical maintenance work at the stack integration unit. Eventually, starting after ∼4200 h in Fig. 2, a final electrochemical characterization was carried out to assess the stack degradation more in detail.

Initial stack performance.—Figure 3 shows the initial *i-V* curve and the measured temperatures in the stack in electrolysis mode. The stack was operated with a total fuel gas flow of 8.2 NLPM consisting of 80% H_2O, 20% H_2. The stack showed an average OCV of 0.904 V per RU at a core temperature T_4 of 730 °C which is in accordance with thermodynamic calculations of the Nernst voltage (also 0.904 V) confirming a good gas-tightness. A non-linear behavior of the *i-V* curve was observed with an almost linear increase of the voltage at low current densities and a flattening of the curve at higher current density values. The initial strong increase coincided with the cooling of the stack temperature due to the endothermic water electrolysis reaction. The Joule heating in the stack increased with current density and therefore, the stack reached isothermal operation at −0.256 A cm^{-2} and an average voltage per RU of 1.244 V. A deviation between the isothermal and the thermoneutral voltage is often observed in real systems due to the heat losses of stack to the environment which usually results in an increased isothermal voltage. In the present case, however, the isothermal voltage is lower than the thermodynamically calculated

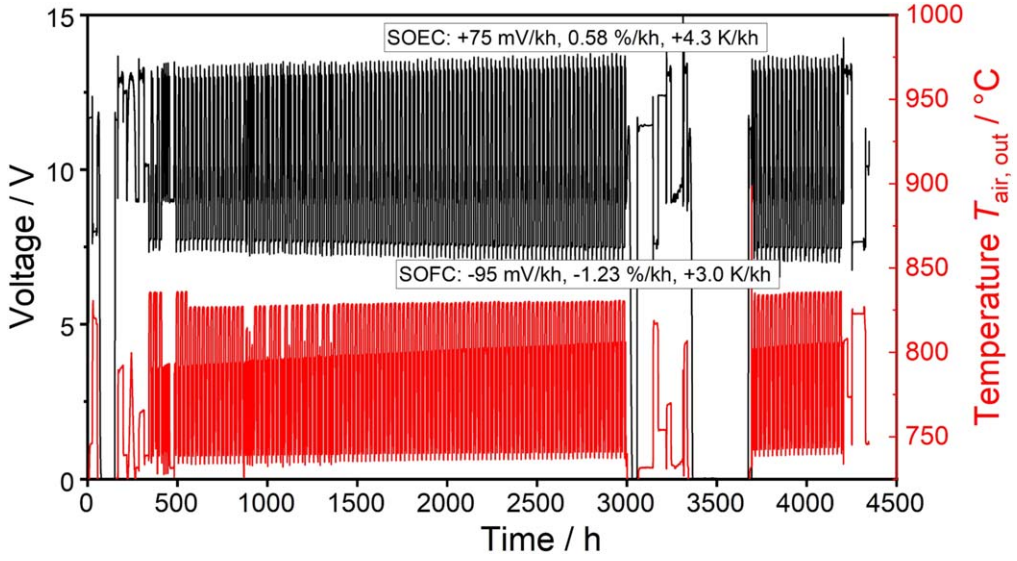

Figure 2. Long-term operation of the stack including 3440 h of reversible SOFC/SOEC cycling.

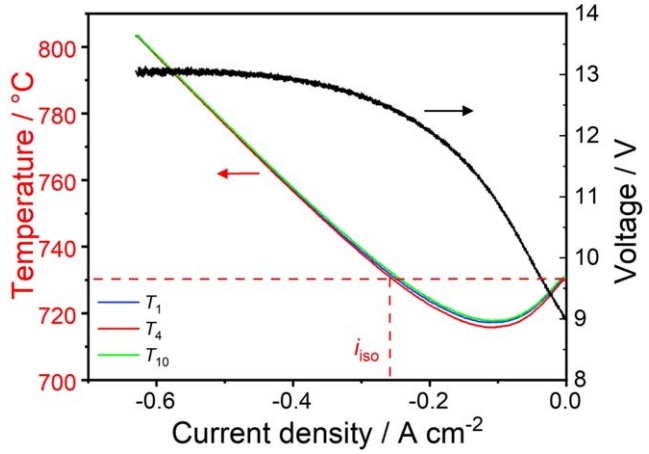

Figure 3. *i-V* curve and temperature evolution of the 10-cell stack in SOEC operation at 80% H_2O, 20% H_2. A steam conversion of 75% was reached at -0.6 A cm^{-2}. At lower current densities, the steam conversion was lower as well. The isothermal current density i_{iso} is indicated for temperature T_4.

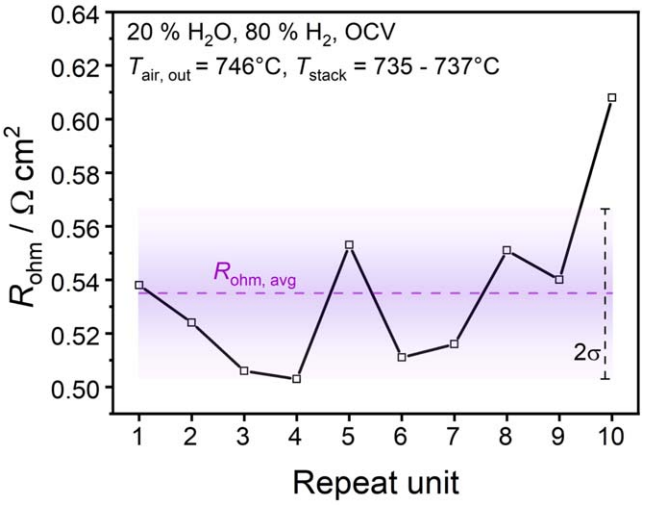

Figure 4. Homogeneity diagram of the ohmic resistance derived from initial EIS measurements at OCV. The purple dashed line indicates the average ohmic resistance value $R_{ohm, avg}$, and the purple rectangle the region of the standard deviation σ.

thermoneutral voltage of 1.284 V at 730 °C. At OCV conditions, the oven temperature of 749 °C is considerably higher than the core temperature of the stack of 730 °C most likely to the low air preheater temperature of 300 °C which cooled down the stack. This discrepancy between stack and oven temperature suggests a heat transfer from the oven environment to the stack to be the reason for the relatively low isothermal voltage. For the determination of the isothermal point, the core temperature T_4 was used. In addition, T_1 and T_{10} in Fig. 3 show a relatively small deviation from the core temperature T_4 indicating a homogeneous temperature distribution over the stack. Above the temperature minimum, the current density increase led to a continuous heating of the stack which eventually entailed a decrease in area-specific resistance (ASR) and a flattening of the *i-V* curve.

Electrochemical characterization of the stack at OCV was performed by means of EIS at the beginning of the test to investigate the ohmic resistance of all RUs under the absence of current. At this operating point the temperature variations over the height of the stack of below 2 K were relatively small and thus, temperature effects on the ohmic resistance distribution can be neglected. A homogeneity diagram with the ohmic resistance is depicted in Fig. 4. The average value was $0.535 \pm 0.032\ \Omega\ cm^2$, and the highest value of $0.608\ \Omega\ cm^2$ in RU 10 showed an increase of ~20% compared to the lowest value of $0.503\ \Omega\ cm^2$ in RU 4. The ohmic resistance is frequently assumed to be governed by the electrolyte resistance which would suggest a 20% thicker electrolyte of RU 10 compared to RU 4. However, more likely the differences in ohmic resistances were caused by different contact resistances of the cells in the stack, e.g. on the air side.

Subsequently, the stack was characterized at the three reference operating points, two in electrolysis and one in fuel cell mode. The initial voltage distribution at equilibrium at all operating points is shown in Fig. 5. Furthermore, the values for ohmic resistance R_{ohm}, polarization resistance R_{pol} and total resistance R_{tot} of all RUs derived from EIS are depicted in Fig. 6. The corresponding average values are given in Table I. At an applied electrical current density of -0.6 A cm^{-2}, the stack produced 5.39 NLPM hydrogen and reached 0.987 kW with an electrical efficiency of 96.8%. At -0.39 A cm^{-2}, the stack generated 3.49 NLPM hydrogen and reached 0.654 kW with an efficiency of 95.9%.

The initial voltage distribution of the two electrolysis reference points at part load and nominal load followed a similar profile with relatively

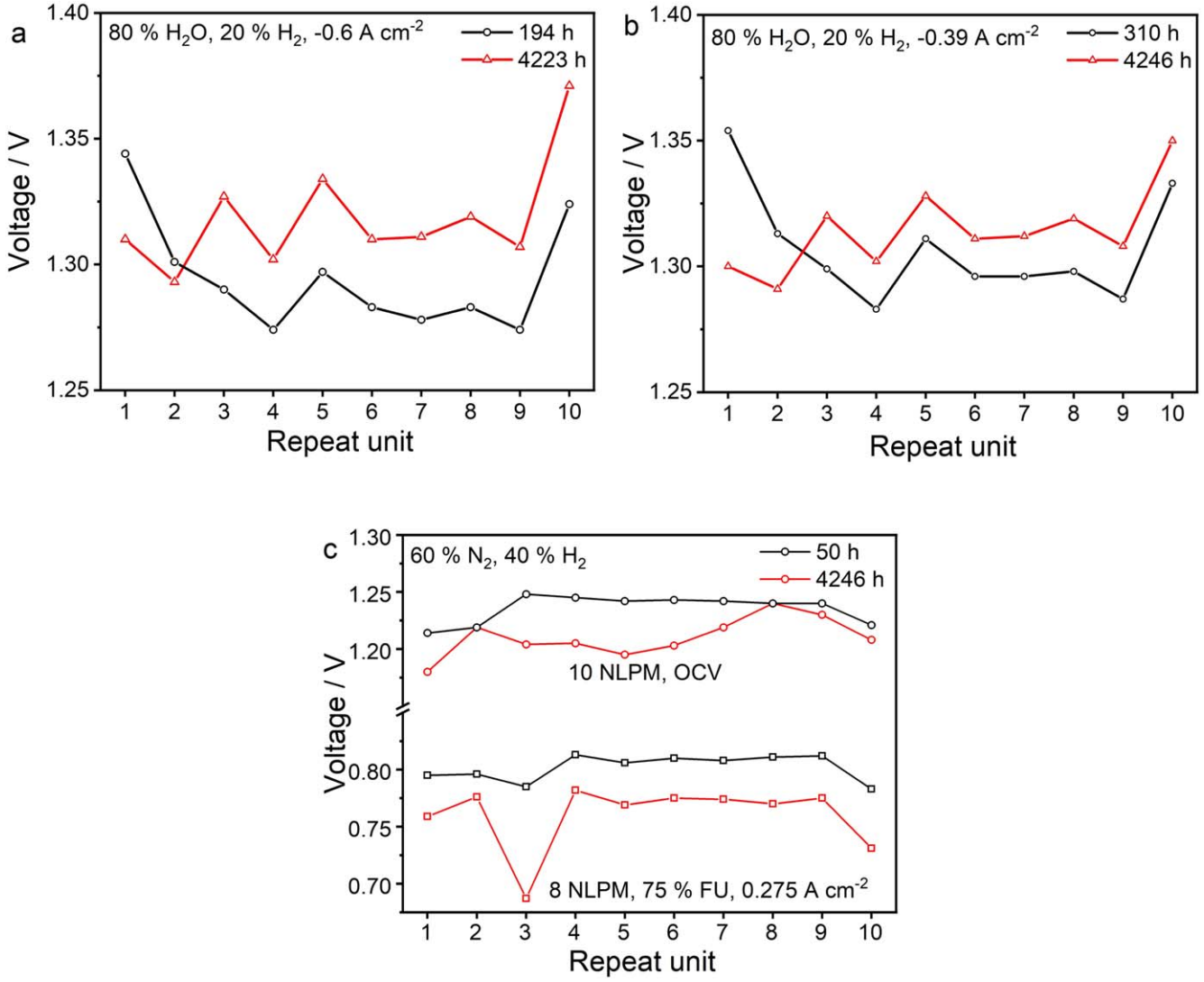

Figure 5. Voltage homogeneity diagram depicting voltage of the RUs inside the stack in SOEC and SOFC with a fuel gas consisting of (a) and (b) 80% H_2O and 20% H_2 and (c) 60% N_2, 40% H_2. Voltage values are shown at (a) -0.6 A cm^{-2} (ELNL), (b) -0.39 A cm^{-2} (ELPL) and (c) 0.275 A cm^{-2} (FCNL)/OCV.

high voltage values for RU 5, RU 8 and RU 10 originating from high ohmic resistance values of these RUs. Both operating points were slightly exothermic, however, in both cases the temperature difference over the height of the stack was below 1 K and thus, the temperature effect on the voltage and resistance distribution should be small. Interestingly, the average voltage value of 1.307 V at -0.39 A cm^{-2} was slightly higher than the 1.295 V at -0.6 A cm^{-2}. Moreover, both ohmic and polarization resistance were significantly greater as well. The main reason for this counterintuitive behavior was the considerable stack heating between these operating points which caused a stack core temperature (T_4) difference of ~30 K (797 °C vs 768 °C), and the associated reduction in resistance of the temperature-activated processes of electrode kinetics, ionic and electronic conductivity. Furthermore, to obtain a constant steam conversion of 75%, the fuel gas flow rate was significantly reduced at part load of -0.39 A cm^{-2} (5.78 NLPM vs 8.2 NLPM) which led to an increase in gas conversion resistance contributing to an increased overall polarization resistance.[20]

Before applying a current for the referencing at the nominal SOFC operating point FCNL, the stack voltage was equilibrated at OCV with 10 NLPM fuel gas consisting of 60% N_2, 40% H_2. The voltage values of all RUs at this operating point were greater than 1.2 V demonstrating the initial high gas-tightness of the stack (see Fig. 5c). At an applied electrical current density of 0.275 A cm^{-2} and with 8 NLM fuel gas flow rate, the stack reached 0.28 kW with an electrical efficiency of 48.8%. Temperatures of 835 °C in RU 4, 831 °C in RU 1 and 833 °C in RU 10 were measured showing a non-uniform temperature distribution inside the stack, which was caused by the so-called "edge effect".[21] During operation, the heat losses at the outer RUs (bottom and top plate) to the surroundings of the stack were higher compared to the RUs in the middle which had lower heat losses. Thus, higher temperatures occurred in the middle cells, which led to generally higher voltage values (Fig. 5c) due to lower ohmic and electrode resistances. The average ohmic resistance of 0.282 Ω cm^2 per RU at this reference point was lower than the ones at the electrolysis reference points due to the higher stack temperatures of 831 °C–835 °C. At the same time, the average polarization resistance of 0.806 Ω cm^2 was considerably higher since the total fuel gas flow rate after the subtraction of inert nitrogen was significantly lower (3.2 NLPM) to achieve the 75% FU resulting in an increased gas conversion resistance.[20] In addition, the gas conversion impedance becomes large if either the steam or the hydrogen partial pressure are low.[9] At the SOFC reference point the steam content at the inlet was low and consequently, the gas conversion impedance dominated the total ASR. Moreover, the gas conversion impedance shows a slight increase with operating temperature.[20]

In particular, the polarization resistances of RU 2 and RU 3 of ~1.2 Ω cm^2 were very high although these RUs did not show a

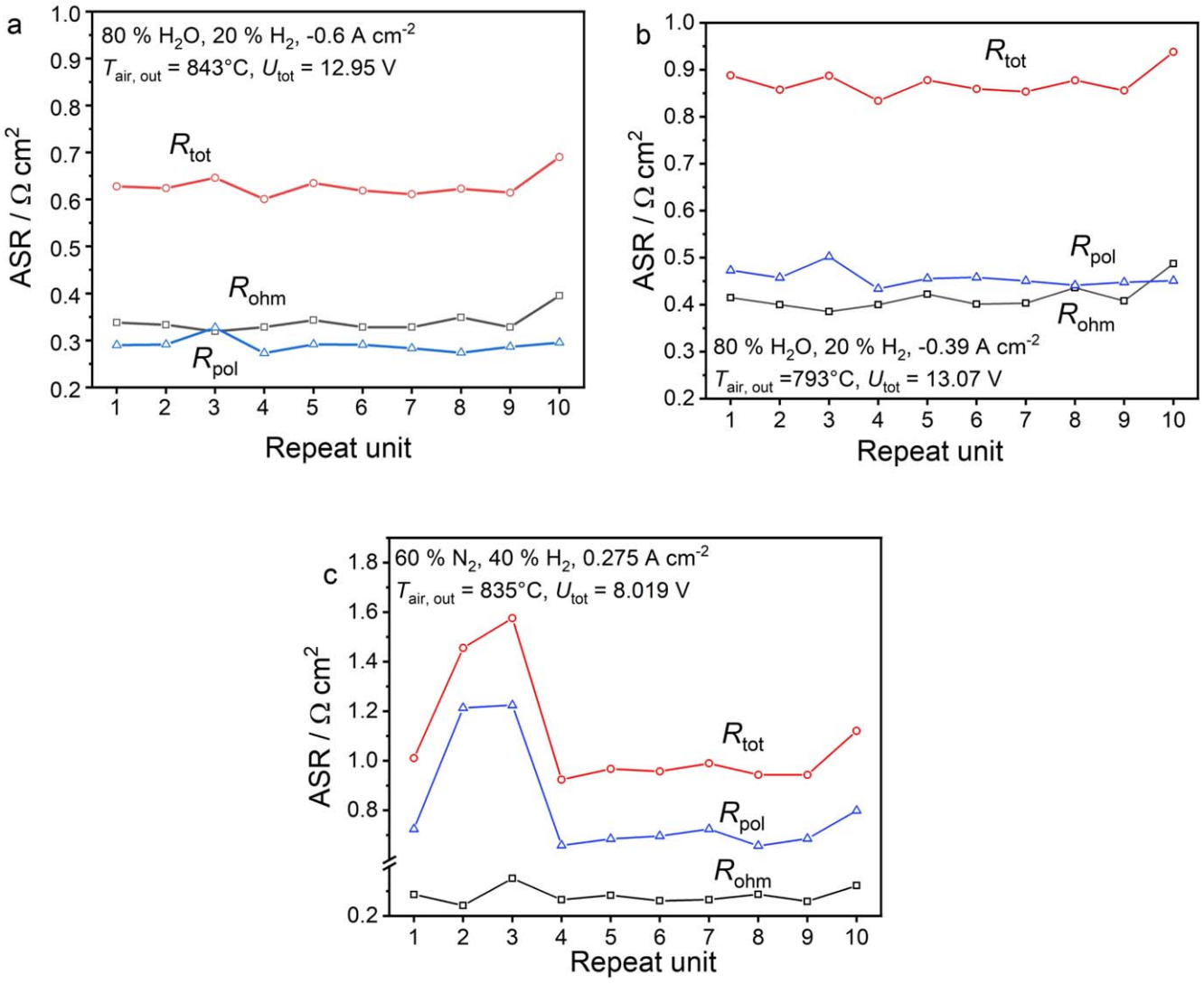

Figure 6. Homogeneity diagram depicting ohmic resistance, polarization resistance and total resistance of the RUs inside the stack in SOEC and SOFC with a fuel gas consisting of (a) and (b) 80% H_2O and 20% H_2 and (c) 60% N_2, 40% H_2. Voltage values are shown at (a) -0.6 A cm^{-2}, (b) -0.39 A cm^{-2} and (c) 0.275 A cm^{-2}/OCV. Temperatures inside the stack were (a) $T_1 = 796.7$ °C, $T_4 = 796.3$ °C, $T_{10} = 796.7$ °C, (b) $T_1 = 767.6$ °C, $T_4 = 767.4$ °C, $T_{10} = 768.0$ °C, (c) $T_1 = 831.3$ °C, $T_4 = 835$ °C, $T_{10} = 833.5$ °C.

Table I. Average values and standard deviation for ohmic resistance R_{ohm}, polarization resistance R_{pol} and total resistance R_{tot} derived from EIS at three operating points.

Operating point	R_{ohm}/Ω cm^2	R_{pol}/Ω cm^2	R_{tot}/Ω cm^2	Average voltage value/V
−0.6 (ELNL)	0.339 ± 0.022	0.29 ± 0.015	0.629 ± 0.025	1.295
−0.39 (ELPL)	0.457 ± 0.019	0.416 ± 0.029	0.873 ± 0.029	1.307
0.275 (FCNL)	0.282 ± 0.033	0.806 ± 0.221	1.088 ± 0.233	0.802

pronounced low operating voltage. The high polarization resistance was mainly due to an increase in resistance at ∼0.1 Hz (see Fig. S1) where indeed the gas conversion impedance is located. Its variation is correlated with the gas flow distribution between the different RUs in the stack, which is the most likely explanation for the observed differences in polarization resistance. Therefore, the increased low frequency response of RU 2 and RU 3 suggests that their gas supply was lower compared to other RUs. Moreover, the imposition of an alternating current signal of 0.015 A cm^{-2} during the EIS measurements added a temporary maximum fuel utilization of 4.1% to the average FU of 75%. Therefore, it is likely that at such high fuel utilization values, the differences in gas flow distribution were even more apparent during the EIS measurements.

Reversible long-term operation.—In Fig. 2, the voltage and air outlet temperature evolution of the stack is shown during the reversible long-term operation between $t = 350$–4200 h. The maximum stack core temperature change within one SOFC/SOEC cycle was ∼120 K with a maximum temporal temperature gradient of 2 K min^{-1} as depicted during the first cycle in Fig. 1. The maximum temperature occurred while operating at the nominal SOFC operating point and the minimum temperature during the transition from

SOFC to SOEC operation indicating that the endothermic electrolysis operating regime was not crossed fast enough to avoid a temporal cooling of the stack. Similarly, during the SOEC to SOFC transition the stack temperature cooled after switching the gases at OCV and increasing the current in electrolysis operation. During the entire reversible operation period, the voltage degradation in SOEC mode was +7.5 mV/kh per RU or +0.58%/kh which corresponds to 12.5 mΩ cm^2/kh. The degradation was accompanied with a temperature increase of 4.3 K/kh. In SOFC mode, a voltage degradation of 9.5 mV/kh per RU or −1.23%/kh with a temperature increase of 3.0 K/kh was observed corresponding to an average ASR increase of 34.5 mΩ cm^2/kh. These degradation rates range among the lowest ones reported for stacks in rSOC operation in literature so far. The higher relative voltage increase in SOFC operation is partially due to the lower initial voltage compared to SOEC operation, but also has mechanistic reasons as shown in the following subchapter.

During the two thermal cycles at $t = 3000$ h and 3340 h, the mechanical pressure on the stack was removed, air manifolds were disassembled and Pt wires were re-welded to the stack unit. These works had some effects on the stack performance that are illustrated in the supporting information (Figs. S2–S4). Firstly, the OCV evolution in Fig. S2 showed no decrease during the initial 3000 h of rSOC operation suggesting that the continuous exposure of the stack to considerable temperature changes did not affect its gas-tightness. However, at the end of the experiment the OCV values of some RUs were below 1.2 V indicating that the gas-tightness was affected (Fig. S2). Most likely this leakage was caused by the release of mechanical compression during the thermal cycle and the re-welding of the Pt wires to the stack during which hot spots could have formed which caused local cracking of the glass sealants.

Secondly, RU 5 showed unusually high gradual degradation in SOEC operation and its voltage already reached 1.54 V at $t = 2990$ h (Fig. S3). However, after the two thermal cycles this voltage increase was recovered to a large extent and the voltage of RU 5 achieved a value of 1.31 V comparable to the average value of the other RUs (see Figs. S3, S4). By contrast, during fuel cell operation, RU 5 neither showed a particularly high degradation nor was it affected by the thermal cycles. We have already observed in our recent work that the contact resistance of the RUs is strongly dependent on temperature and possibly also electrical bias.[18] Since these parameters were different in SOEC and SOFC operation in the present work, it is hypothesized that the strong degradation and its reversal during SOEC operation is related to the loss and subsequent self-healing of the contacting of the RU on the air side under these particular operating conditions.

Thirdly, RU 2 and RU 3 showed a significant increase and decrease of their voltages, respectively, after the thermal cycles. Most likely, the decrease in RU3 was related to the compromised gas-tightness in the stack and a change of the gas flow distribution in the stack due to the maintenance work on the stack assembly which caused an increase in gas conversion for RU 3 and will be further addressed in the following.

These changes also caused a shift of the stack core temperature. During SOFC operation, T_4 increased by ∼6 K after the two thermal cycles reflecting the reduced stack gas-tightness and the corresponding hydrogen chemical oxidation inside the stack. In the meantime, T_4 decreased by 3 K in SOEC operation. This contrary behavior most likely originates from the reduced hydrogen oxidation at lower hydrogen partial pressures in electrolysis and the reduction of the overpotential of RU 5 after the thermal cycles due to contact healing causing lower Joule heating in vicinity of the thermocouple.

Final stack characterization.—For a more detailed understanding of the degradation behavior of the RUs over the height of the stack, their voltage over time at part load and full load in electrolysis and at nominal load in fuel cell mode is depicted in Fig. 5. At the two electrolysis operating points the voltage of nearly all RUs increased considerably in a mostly homogeneous manner. Only RU 1 and RU 2 showed a voltage decrease over time. A detailed analysis of their voltage behavior has shown a significant improvement of the voltage of both RUs after ∼350 h which was possibly due to an initial increase of contacting area. The stack showed an increased voltage degradation rate of 0.5%/kh for the nominal load electrolysis operating point ELNL at −0.6 A cm^{-2} compared to 0.15%/kh at the part load operating point ELPL at −0.39 A cm^{-2} (Table II). The degradation rate at the nominal load electrolysis point was the same as previously reported for the same stack type.[22]

This is in contrast to our previous work where a stack of the same design was investigated for a similar time period in pure steam electrolysis and characterized at the same operating points.[18] In pure steam electrolysis, the stack had shown a negative voltage degradation rate of −0.3%/kh at nominal full load of −0.6 A cm^{-2}, whereas at part load of −0.39 A cm^{-2} a significantly increased rate of 0.5%/kh had been observed.

At the SOFC nominal load reference point, the voltage degradation rate amounted to −1.5%/kh which is close to the −1.23%/kh observed during transient reversible operation (see Fig. 2). Another measurement of the different RU voltages was carried out in SOFC mode with all operating conditions being the same except the oven temperature which was decreased by 12 K to adjust the air outlet temperature to 835 °C. This temperature-correction was performed for internal referencing and led to a slightly increased degradation rate of −1.8%/kh.

Compared to our recent degradation study in steam electrolysis (see Table II), in the present work the degradation rates were higher at −0.6 A cm^{-2} in electrolysis, but lower at −0.39 A cm^{-2} in electrolysis and at 0.275 A cm^{-2} in fuel cell operation.

Based on the results presented so far, it can be concluded that even under potentially severely detrimental rSOC operating

Table II. Overview of different degradation rates determined based on the voltage distribution at the different reference points in rSOC operation and in pure steam electrolysis.

	Operating point	Average voltage degradation rate/mV/kh/RU	Average ASR degradation rate/mΩ cm^2/kh/RU	Initial stack core temperature/°C
rSOC operation	−0.6 A cm^{-2} (ELNL)	+6.5 (+0.5%/kh)	+10.8	796
	−0.39 A cm^{-2} (ELPL)	+2 (+0.15%/kh)	+5.2	767
	0.275 A cm^{-2} (FCNL)	−11.9 (−1.5%/kh)	+43.4	835
	0.275 A cm^{-2} (temperature-corrected)	−14.8 (−1.8%/kh)	+53.8	835
Steam electrolysis operation[18]	−0.6 A cm^{-2} (ELNL)	−4.5 (−0.3%/kh)	−7.5	789
	−0.39 A cm^{-2} (ELPL)	+6.8 (+0.4%/kh)	+17.8	763
	0.275 A cm^{-2} (temperature-corrected)	−20 (−2.5%/kh)	+72.7	835

conditions, the degradation of MK35x stacks rate was mitigated close to or even below the value of +0.5%/kh target by the Strategic Research & Innovation Agenda from the Clean Hydrogen Joint Undertaking by 2030 for solid oxide electrolysis,[23] and is in the same range as the lowest values reported for stacks operated in steam electrolysis. For example, different durability tests over >1000 h of electrolyte-supported cell-based stacks showed relative voltage increase rates of 0.5%−0.6%/kh.[9,11,24] Degradation rates of stacks with fuel electrode supported cells were frequently reported to be higher,[25–29] but some studies observed degradation rates of 0.5%–0.7%/kh as well.[30–32] Some other long-term degradation studies prefer to use the ASR increase over time as a more accurate measure of degradation.[9,11,24,25,33] Values of 12–18 mΩ cm^2/kh were reported for stacks with ESC,[9,11,24,25,34] and 20 mΩ cm^2/kh for stacks with metal-supported cells.[33]

However, the degradation rate during SOFC operation was significantly increased. For example, a previous long-term test of MK351 stack in fuel cell operation for more than 20,000 h has shown an average voltage decrease of only −0.7%/kh.[14] In general, SOFC degradation rates of 0.2%/kh are targeted for 2030 by the Clean Hydrogen Joint Undertaking and values of 0.1%–0.3%/kh were reported for stacks with metal-supported,[35,36] fuel electrode supported[37–40] and electrolyte-supported cells.[34,41]

For a more in-depth understanding of the degradation behavior, the impedance spectra at −0.39 A cm^{-2} and −0.6 A cm^{-2} in SOEC operation and 0.275 A cm^{-2} in SOFC operation at the beginning and the end of the experiment were analyzed and the ohmic resistance, polarization resistance and total resistance degradation rates were determined (Fig. 7). The average degradation rates per RU and values derived from the previous steam electrolysis long-term test[18] are summarized for comparison in Table III as well. In accordance with the similar voltage evolution in Fig. 5, the different resistance degradation rates show a similar behavior at the two electrolysis reference points. Under both conditions, the ohmic resistance increased over time and the polarization decreased resulting in a net increase of the total resistance. At −0.39 A cm^{-2} the total degradation rate was 29.7 mΩ cm^2/kh/RU and therefore, higher than the 18 mΩ cm^2/kh/RU observed at −0.6 A cm^{-2} which was mainly due to a similarly increased ohmic resistance degradation rate per RU of 38.9 mΩ cm^2/kh or 9.4%/kh compared to 25.1 mΩ cm^2/kh or 7.4%/kh. By contrast, the polarization resistance per RU decreased by 7.0 mΩ cm^2/kh or by 2.4%/kh at −0.6 A cm^{-2} and 9.8 mΩ cm^2/kh or by 2.1%/kh at −0.39 A cm^{-2}. As shown in representative EIS measurements of RU 4 in Fig. 8, the polarization resistance at both conditions showed a pronounced activation in the frequency range of ∼10 Hz similar to the behavior observed during pure steam electrolysis operation,[18] while the impedances at other frequencies remained largely unaffected over time. At this frequency range, most likely the LSMM'/ScSZ oxygen electrode and a Ni/CGO surface process are present.[42] As already discussed in our previous work, the reason for this behavior is unclear, but it is hypothesized to originate from an activation of the LSMM' perovskite possibly due to the removal of SrO species from the surface and enhanced oxygen vacancy formation.[18,43]

At the SOFC operating point, the stack showed the highest total degradation rate of 38.7 mΩ cm^2/kh per RU (+3.9%/kh) despite displaying the highest stack core temperature (Table III). Here, the relative ohmic resistance degradation rate of 12.7%/kh was substantially increased compared to the SOEC operating points. The ohmic resistance of the SOC is frequently assumed to be governed by the ionic resistance of the doped zirconia electrolyte,[44,45] and degradation rates of the ionic conductivity of the Sc-doped zirconia of up to 10%/kh have been reported in the past which are exceeded by some of the values observed in the present study.[46,47] Moreover, in our previous work we already suggested that other processes most likely contribute significantly to the ohmic resistance as well, such as loss of contact area on the air side or the formation of oxide scales on the interconnect.[18] For example, the contact resistance evolution of contacting solutions on the air side is discussed in Ref. 48. The activation energy barriers for the electronic conductivity in the oxygen electrode perovskite used for current collection (<0.6 eV), electronic conductivity in the chromium oxide scales on the interconnect (0.78 eV) and ionic conductivity in the 10Sc1CeSZ (0.86 eV) show significant differences. Since the stack temperature was different at all three operating points as well, the contributions of the different loss processes to the ohmic resistances are expected to vary. In our previous work, we suggested contact healing at the oxygen electrode at higher operating temperatures to be the reason for the decreased degradation rates at nominal electrolysis load of −0.6 A cm^{-2} compared to part load of −0.39 A cm^{-2} (see Table III). However, such a phenomenon cannot fully explain the behavior observed in the present work since the SOFC operating point showed the largest relative ohmic resistance while being operated at the highest temperature.

Interestingly, the EIS measurements at the SOFC operating conditions (Figs. 8e–8f) did not show a change at frequencies ∼10 Hz, and only a marginal improvement at ∼2 Hz. At the same time, the gas conversion resistance at frequencies of ∼0.5 Hz slightly increased most likely due to an effective reduction of the hydrogen fuel flow rate due to chemical oxidation in the stack which was reflected by a decrease in OCV. The increase in gas conversion resistance and the absence of a substantial reduction in LSMM' oxygen electrode resistance caused an average positive polarization resistance degradation rate of 3.8 mΩ cm^2/kh/RU (+0.5%/kh).

Hence, a substantial difference in LSMM'/ScSZ oxygen electrode behavior is observed over time depending on the operating mode which could also be the reason for the rather large relative increase of the ohmic resistance during SOFC operation. One potential reason could be a considerable effect of the electrical bias on the vacancy concentration in the LSMM' perovskite which might influence its electro-catalytic activity. However, a more detailed understanding of the fundamental LSMM'/ScSZ electrode behavior is required to fully explain the mechanistic reasons for the observed degradation.

Finally, ohmic, polarization and total resistance degradation rates at part load of −0.39 A cm^{-2} during reversible cycling can also be compared to the ones obtained during the previous long-term test in steam electrolysis (Table III). The average ohmic resistance degradation rate of 38.9 mΩ cm^2/kh/RU in rSOC operation was significantly lower than the 58.2 mΩ cm^2/kh/RU in steam electrolysis operation. At −0.6 A cm^{-2}, the ohmic resistance degradation rate of 25.1 mΩ cm^2/kh/RU in rSOC operation was lower than the 39.5 mΩ cm^2/kh/RU in steam electrolysis. In addition, another set of rSOC degradation rates was calculated based on additional EIS measurements at −0.39 A cm^{-2} recorded at an intermediate operation time point of 3421 h. At this point, the ohmic resistance degradation rate of 55.1 mΩ cm^2/kh/RU was very similar to the one in steam electrolysis and is probably a more accurate measure of the stack degradation since it was determined before the maintenance work which had caused changes in contacting and gas-tightness of the stack as described above.

The polarization resistance degradation rate at −0.39 A cm^{-2} of −9.8 mΩ cm^2/kh/RU (or −14.3 mΩ cm^2/kh/RU for the intermediate EIS measurement at 3421 h) showed a significantly lower value in rSOC operation compared to the −24.3 mΩ cm^2/kh/RU in steam electrolysis. Since the activation of the oxygen electrode is most likely restricted to the operation of the stack in steam electrolysis, the difference in polarization resistance degradation rates might be explained by the lower overall time in steam electrolysis operation during the rSOC test.

Eventually, the rSOC test showed a total resistance degradation rate of 29.7 mΩ cm^2/kh/RU at −0.39 A cm^{-2} for the whole test, and 40.8 mΩ cm^2/kh/RU if only the intermediate EIS measurement is considered which is either lower or higher than the 33.8 mΩ cm^2/kh/RU determined in pure steam electrolysis.

Thus, summing up based on the presented results no clear indications for a generally increased overall degradation in either rSOC or steam electrolysis operation could be found for the

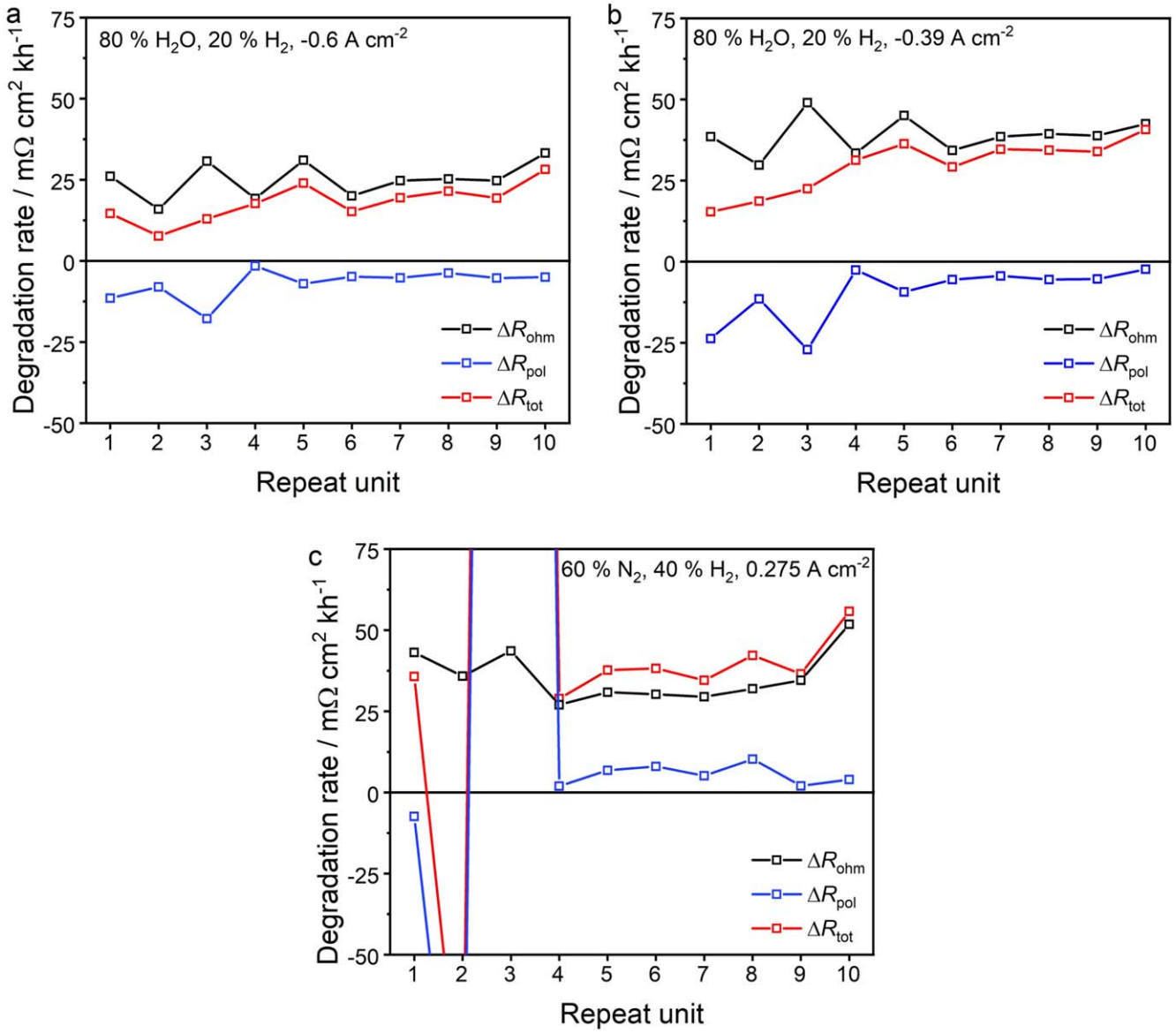

Figure 7. Degradation rates of ohmic, polarization and total resistance derived from EIS for the three reference points. (c) Polarization and total resistance values of RU 2 and RU 3 are outside the window for enhanced visibility. ΔR_{pol} and ΔR_{tot} for RU 2 were −140 mΩ cm^2/kh/RU and −104 mΩ cm^2/kh/RU, respectively. ΔR_{pol} and ΔR_{tot} for RU 3 were 983 mΩ cm^2/kh/RU and 1026 mΩ cm^2/kh/RU, respectively.

Table III. For average value calculation of polarization and total resistance at the SOFC operating point of the rSOC test, RU 2 and RU 3 where ignored due to their strong change in gas conversion resistance that were most likely caused by the manual work during technical maintenance.

		R_{ohm} [mΩ cm^2/kh/RU]	R_{pol} [mΩ cm^2/kh/RU]	R_{tot} [mΩ cm^2/kh/RU]	Initial temperature in stack [°C]
rSOC	0.275 A cm^{-2}	35.8 (+12.7%/kh)	3.8 (+0.5%/kh)	38.7 (+3.9%/kh)	835
	−0.6 A cm^{-2}	25.1 (+7.4%/kh)	−7.0 (−2.4%/kh)	18.0 (+2.9%/kh)	796
	−0.39 A cm^{-2} (total)	38.9 (+9.4%/kh)	−9.8 (−2.1%/kh)	29.7 (+3.4%/kh)	767
	−0.39 A cm^{-2} (until 3421 h)	55.1 (+13.2%/kh)	−14.3 (−3.1%/kh)	40.8 (+4.7%/kh)	767
Steam electrolysis	−0.6 A cm^{-2}	39.5	—	—	789
	−0.39 A cm^{-2}	58.2	−24.3	33.8	763

investigated operating conditions. The degradation rates calculated in SOFC mode seem high, however, detailed long-term data for the same stack type are unfortunately not available for comparison. These results demonstrate the high maturity of the MK35x stack technology whereas a previous test of a 30-cell stack based on electrolyte supported cells and Crofer22APU interconnects had shown a significant increase in degradation and, in particular, ohmic resistance once the stack was operated reversibly with comparable SOFC/SOEC cycles.[9] The high stability in the present work could potentially be related to the smaller stack size and the high

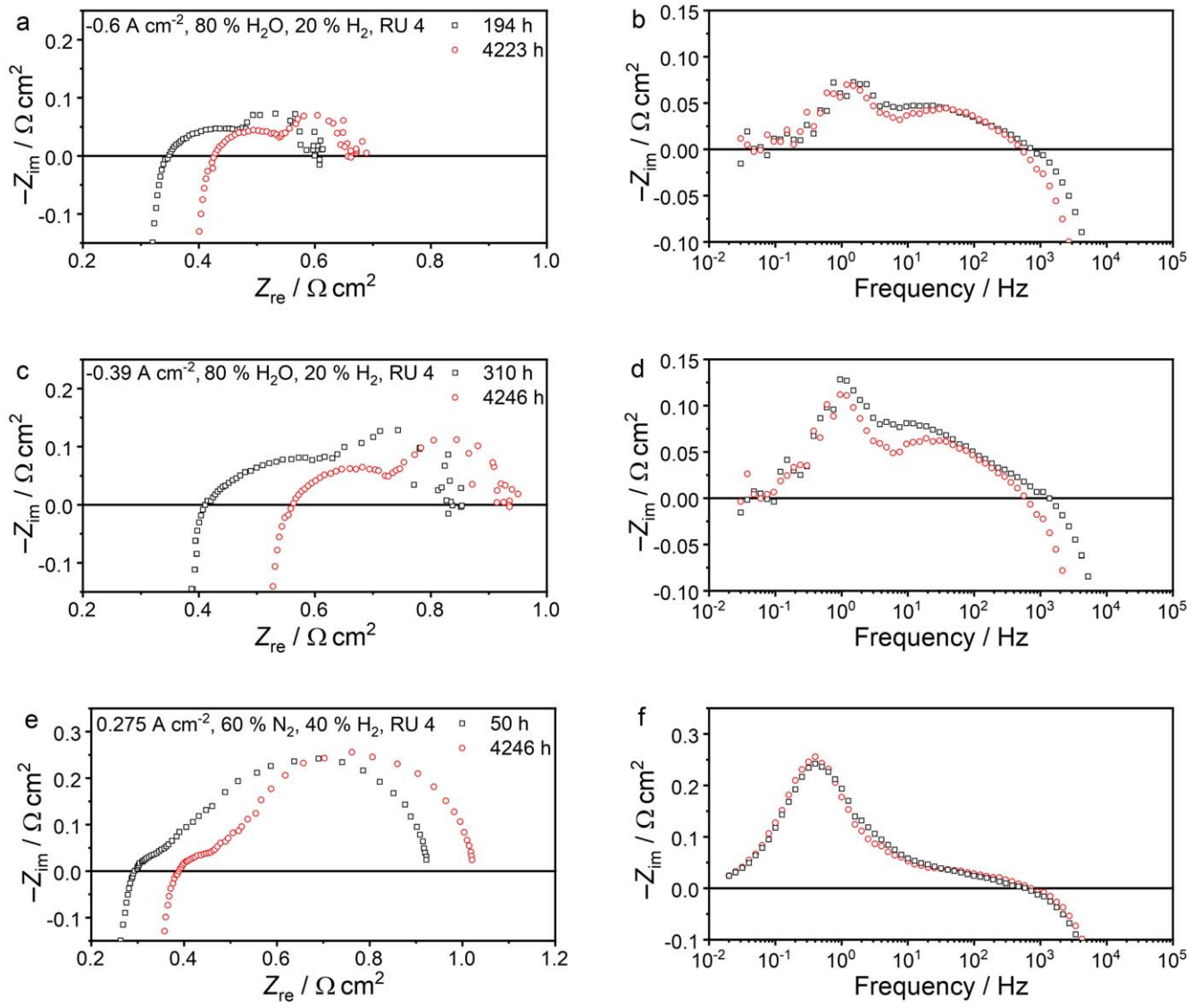

Figure 8. (a) Nyquist plot, (b) imaginary impedance plot of representative EIS spectra of RU 4 in electrolysis operation with gas composition consisting of 80% H_2O and 20% H_2 at -0.6 A cm^{-2}, (c) Nyquist plot, (d) imaginary impedance plot of EIS spectra of RU 4 in electrolysis operation with gas composition consisting of 80% H_2O and 20% H_2 at -0.39 A cm^{-2}, (e) Nyquist plot, (f) imaginary impedance plot of representative EIS spectra of RU 4 in fuel cell operation with gas composition consisting of 60% N_2 and 40% H_2 at -0.275 A cm^{-2}.

thermal conductivity of the CFY interconnects of 35–45 W m^{-1} K^{-1} (20 °C–900 °C) which lead to a rather homogeneous temperature and current distribution and could diminish thermal stresses inside the stack.[11] However, the determined degradation rates in the present work were also considerably impacted by an initially large increase of the ohmic resistance and a simultaneous decrease of the oxygen electrode resistance. The changes of both resistance contributions can be expected to level off over time and durability experiments with even longer testing times will be necessary to better compare the stack technology's long-term stability to other literature values.

Summary and Conclusions

In the present study, the degradation behavior of an electrolyte-supported cell-based "MK35x" stack was investigated during reversible operation for more than 3400 h with 137 SOFC/SOEC cycles each of 24 duration with a maximum temporal temperature gradient of ±2 K min^{-1}. Voltage degradation rates of +0.58%/kh and −1.23%/kh were determined in electrolysis and fuel cell operation, respectively, which are among the lowest ones reported in literature so far. The higher degradation rate in fuel cell operation was due to a higher relative increase of both ohmic and polarization resistance. A hypothesis for the high ohmic resistance in fuel cell operation is the complex influence of temperature and electrical bias on the contacting of the oxygen electrode. Moreover, during electrolysis operation, a decrease of the LSMM'/ScSZ oxygen electrode resistance was observed over time indicating an activation behavior of the electrode. However, no such activation behavior was witnessed during fuel cell operation with the mechanistic reason being unclear. The OCV decreased only due to manual maintenance work on the stack integration, while staying constantly high during the actual long-term operation. Comparison to a previously published long-term test in steam electrolysis showed no indications for an increased degradation during rSOC operation. A post test analysis will be carried out in future work to correlate the electrochemically observed degradation behavior with microstructural and physico-chemical phenomena.

Acknowledgments

The German Ministry of Education and Research (BMBF) is acknowledged for funding in the framework of the "SOC-Degradation 2.0" project under grant number 03SF0621B.

ORCID

Matthias Riegraf https://orcid.org/0000-0002-0383-2545
Michael Lang https://orcid.org/0000-0001-7756-9658
Rémi Costa https://orcid.org/0000-0002-3534-1935

References

1. H. Ritchie, M. Roser, and P. Rosado, *Renewable Energy' Published online at OurWorldInData.org. Retrieved from:* (2020), https://ourworldindata.org/renewable-energy [Online Resource].
2. P. A. Kempler, J. J. Slack, and A. M. Baker, *Joule*, **6**, 280 (2022).
3. M. Riegraf, R. Costa, and K. A. Friedrich, "Electrolyzer – Solid Oxide Electrolyzer | Overview." *Encyclopedia of Electrochemical Power Sources (Second Edition)* (Elsevier, Amsterdam), p. 109 (2025).
4. G. Schiller, M. Lang, P. Szabo, N. Monnerie, H. von Storch, J. Reinhold, and P. Sundarraj, *J. Power Sources*, **416**, 72 (2019).
5. C. Wulf, P. Zapp, and A. Schreiber, *Frontiers in Energy Research*, **8**, 191 (2020).
6. O. Posdziech, K. Schwarze, and J. Brabandt, *Int. J. Hydrogen Energy*, **44**, 19089 (2019).
7. C. Graves, S. D. Ebbesen, S. H. Jensen, S. B. Simonsen, and M. B. Mogensen, *Nat. Mater.*, **14**, 239 (2015).
8. M. Lang, Y. Lee, I. Lee, P. Szabo, J. Hong, J. Cho, and R. Costa, *J. Electrochem. Soc.*, **170**, 114516 (2023).
9. M. Lang, S. Raab, M. S. Lemcke, C. Bohn, and M. Pysik, *Fuel Cells*, **20**, 690 (2020).
10. A. Wood, H. He, T. Joia, and C. C. Brown, *ECS Trans.*, **66**, 23 (2015).
11. S. Megel et al., *ECS Trans.*, **78**, 3089 (2017).
12. M. Kusnezoff, M. Jahn, S. Megel, E. Reichelt, N. Trofimenko, G. Herz, W. Beckert, J. Schilm, A. Rost, and J. Schoene, *ECS Trans.*, **103**, 307 (2021).
13. M. Kusnezoff, S. Megel, C. Rix, P. Adam, E. Reichelt, G. Herz, M. Jahn, N. Trofimenko, and A. Michaelis, *ECS Trans.*, **91**, 2579 (2019).
14. C. Bienert, M. Brandner, S. Skrabs, A. Venskutonis, L. S. Sigl, S. Megel, W. Becker, N. Trofimenko, M. Kusnezoff, and A. Michaelis, *ECS Trans.*, **68**, 2159 (2015).
15. S. Megel, C. Dosch, S. Rothe, M. Kusnezoff, N. Trofimenko, V. Sauchuk, A. Michaelis, C. Bienert, M. Brandner, and A. Venskutonis, *ECS Trans.*, **57**, 89 (2013).
16. N. Trofimenko, M. Kusnezoff, and A. Michaelis, *ECS Trans.*, **35**, 315 (2011).
17. S. Megel, M. Kusnezoff, N. Trofimenko, V. Sauchuk, A. Michaelis, A. Venskutonis, K. Rissbacher, W. Kraussler, M. Brandner, and C. Bienert, *ECS Trans.*, **35**, 269 (2011).
18. M. Riegraf, P. Szabo, M. Lang, R. Costa, S. Rothe, S. Megel, and M. Kusnezoff, *J. Electrochem. Soc.*, **171**, 054504 (2024).
19. N. Trofimenko, M. Kusnezoff, S. Mosch, and A. Michaelis, *ECS Trans.*, **91**, 263 (2019).
20. W. G. Bessler and S. Gewies, *J. Electrochem. Soc.*, **154**, B548 (2007).
21. M. Lang, C. Auer, G. Braniek, F. Wenz, and F. Hauler, *ECS Trans.*, **68**, 2441 (2015).
22. S. Megel, C. Dosch, S. Rothe, C. Folgner, N. Trofimenko, A. Rost, M. Kusnezoff, E. Reichelt, M. Jahn, and A. Michaelis, *ECS Trans.*, **78**, 3089 (2017).
23. Clean Hydrogen Joint Undertaking, Strategic Research and Innovation, Agenda 2021—2027 Accessed October 2024 https://clean-hydrogen.europa.eu/system/files/2022-02/Clean%20Hydrogen%20JU%20SRIA%20-%20approved%20by%20GB%20-%20clean%20for%20publication%20%28ID%2013246486%29.pdf.
24. M. Riedel, M. P. Heddrich, and K. A. Friedrich, *Fuel Cells*, **20**, 592 (2020).
25. J. Aicart, L. Tallobre, A. Surrey, B. Gervasoni, C. Geipel, H. Fontaine, S. Desousanobre, and J. Mougin, *Int. J. Hydrogen Energy*, **60**, 531 (2024).
26. D. Schäfer, Q. Fang, L. Blum, and D. Stolten, *J. Power Sources*, **433**, 126666 (2019).
27. G. Corre and A. Brisse, *ECS Trans.*, **68**, 3481 (2015).
28. J. Aicart, A. Surrey, L. Champelovier, K. Henault, C. Geipel, O. Posdziech, and J. Mougin, *Fuel Cells*, **23**, 463 (2023).
29. J. Mougin, A. Chatroux, K. Couturier, M. Petitjean, M. Reytier, G. Gousseau, and F. Lefebvre-Joud, *Energy Procedia*, **29**, 445 (2012).
30. Q. Fang, L. Blum, and N. H. Menzler, *J. Electrochem. Soc.*, **162**, F907 (2015).
31. Q. Fang, C. E. Frey, N. H. Menzler, and L. Blum, *J. Electrochem. Soc.*, **165**, F38 (2018).
32. G. Rinaldi, S. Diethelm, E. Oveisi, P. Burdet, J. Van Herle, D. Montinaro, Q. Fu, and A. Brisse, *Fuel Cells*, **17**, 541 (2017).
33. P. Hjalmarsson, J. Harman, C. Macauley, I. Methley, J. Ryley, A. Zerfa, C. Hargrove, and M. Selby, *ECS Trans.*, **111**, 977 (2023).
34. C. Geipel, K. Hauptmeier, K. Herbrig, F. Mittmann, M. Münch, M. Pötschke, L. Reichel, T. Strohbach, T. Seidel, and A. Surrey, *ECS Trans.*, **91**, 123 (2019).
35. R. T. Leah, A. Bone, A. Selcuk, M. Rahman, A. Clare, M. Lankin, F. Felix, S. Mukerjee, and M. Selby, *ECS Trans.*, **91**, 51 (2019).
36. R. Leah et al., *ECS Trans.*, **103**, 679 (2021).
37. Q. Fang, U. de Haart, D. Schäfer, F. Thaler, V. Rangel-Hernandez, R. Peters, and L. Blum, *J. Electrochem. Soc.*, **167**, 144508 (2020).
38. K. Asano, T. Imabayashi, A. Ido, H. Morita, T. Yamamoto, and Y. Mugikura, *ECS Trans.*, **111**, 155 (2023).
39. M. Yoshikawa, T. Yamamoto, K. Asano, K. Yasumoto, and Y. Mugikura, *ECS Trans.*, **68**, 2199 (2015).
40. B. P. Borglum and H. Ghezel-Ayagh, *ECS Trans.*, **68**, 89 (2015).
41. A. Mai, J. G. Grolig, M. Dold, F. Vandercruysse, R. Denzler, B. Schindler, and A. Schuler, *ECS Trans.*, **91**, 63 (2019).
42. M. Riegraf, M. P. Hoerlein, R. Costa, G. Schiller, and K. A. Friedrich, *ACS Catal.*, **7**, 7760 (2017).
43. S. P. Jiang, *J. Mater. Sci.*, **43**, 6799 (2008).
44. J. Kondoh, T. Kawashima, S. Kikuchi, Y. Tomii, and Y. Ito, *J. Electrochem. Soc.*, **145**, 1527 (1998).
45. F. T. Ciacchi and S. P.-S. Badwal, *J. Eur. Ceram. Soc.*, **7**, 197 (1991).
46. S. Omar, W. B. Najib, and N. Bonanos, *Solid State Ionics*, **189**, 100 (2011).
47. M. R. Terner, J. A. Schuler, A. Mai, and D. Penner, *Solid State Ionics*, **263**, 180 (2014).
48. M. Brandner, C. Bienert, S. Megel, M. Kusnezoff, N. Trofimenko, V. Sauchuk, A. Venskutonis, W. Kraussler, A. Michaelis, and L. S. Sigl, *ECS Trans.*, **57**, 2235 (2013).